Electrical Engineering (2020) 102:1593–1604
https://doi.org/10.1007/s00202-020-00978-9

ORIGINAL PAPER

Wavelet transform-based protection of transmission line incorporating SSSC with energy storage device

H. V. Gururaja Rao[1] · Nagesh Prabhu[2] · R. C. Mala[1]

Received: 2 July 2019 / Accepted: 13 March 2020 / Published online: 21 March 2020

Abstract
Series compensation is generally used with long transmission lines to increase power transfer through the line and to enhance system stability. In the case of voltage source converter-based series flexible AC transmission system (FACTS) controller, an energy storage device can be incorporated at the DC bus which further improves control of real and reactive power flow. However, four-quadrant operation of FACTS controllers with energy storage device poses new challenges for the operation, control and protection of power system. Most commonly used protection scheme for long transmission lines, the distance relay, may not be reliable in case of lines compensated with series FACTS controllers. This paper proposes a new wavelet transform-based relay logic for fast and reliable detection, and classification of faults in a hybrid series-compensated long transmission line incorporating a passive series capacitor and static synchronous series compensator with energy storage device (SSSC-ES). The proposed relay logic is also able to accurately estimate the location of fault, and a wavelet transform-based boundary condition is used to discriminate between internal and external faults. It is shown through various simulation case studies that the four-quadrant operation of SSSC and fault resistance have negligible impact on the performance of the wavelet transform-based relay.

Keywords Line protection · Wavelet transform · SSSC · Energy storage · Fault index

1 Introduction

Series compensation is generally used with long transmission lines to increase the power transfer through the line and improve stability. Static synchronous series compensator (SSSC) is a series-connected VSC-based FACTS controller which has advantages over variable impedance-type FACTS controller like better technical characteristics, compact, wide range of operation and provision to include an energy storage device at the DC bus [1, 2]. Conventional phase comparison method of protection can be used to protect series-compensated transmission lines [3]. This method helps in discriminating between internal and external faults. The method will not be able to predict the fault location, and it does not provide backup protection for through faults. Distance protection is one of the most widely used methods for the protection of transmission lines [4]. However, emulated impedance of FACTS controllers modifies the impedance seen by the distance relay and hence can cause the distance relay to under-reach or over-reach [5, 6]. Adaptive relay setting is proposed as the solution to overcome mal-operation of distance relay for lines with FACTS controllers [7–9]. However, when energy storage device like fuel cell, battery or super conducting magnetic energy storage (SMES) is connected at the DC bus of SSSC, operating range of SSSC is much broader and covers all the four quadrants. Reactance and resistance emulated by SSSC significantly depend on the operating mode of SSSC [10], and adaptive relay setting to cover the entire operating range of SSSC will be very challenging and may not be practically feasible.

When fault occurs on a transmission line, it initiates a transition condition. Fault current and voltage signals will have transient component which lasts for a short duration.

✉ H. V. Gururaja Rao
gururaj.rao@manipal.edu

Nagesh Prabhu
prabhunagesh@nitte.edu.in

R. C. Mala
mala.rc@manipal.edu

[1] Department of Electrical and Electronics Engineering, Manipal Institute of Technology, Mahe, India

[2] Department of Electrical and Electronics Engineering, NMAM Institute of Technology, Nitte, India

Methods based on mathematical morphology [11, 12] are presented for the protection of transmission lines. Also, transient current and voltage signals contain useful information in the form of high-frequency components which can be used for fault detection. Thus, alternate methods are proposed for the detection of faults in transmission lines based on the presence of high-frequency components in the fault current and/or voltage signals using wavelet transform. In [13], current and voltage signals at both the ends of line are utilized for wavelet-based fault detection and classification. Effect of fault resistance is considered. However, threshold value is different for different values of fault resistance, and hence adaptive threshold value selection is proposed which may be difficult to implement practically. Summation of wavelet detail coefficients is used for fault detection and classification in [14]. Impact of fault resistance on relay performance is not described, and fault location is not estimated. In [15], wavelet transform-based technique is proposed for fault detection and classification. However, for fault location estimation, ANN-based technique is proposed which increases the complexity for practical implementation. Support vector machine technique for the wavelet generated signals is used to detect, classify and locate faults in [16]. Complexity of the algorithm increases with SVM technique, and hence practical implementation becomes complex. Wavelet singular entropy method is proposed for fault detection and classification in [17]. However, fault location is not estimated and effect of fault resistance is not investigated. It should also be noted that mathematical morphology and discrete wavelet transform (DWT)-based methods to detect and classify faults in case of uncompensated lines are presented in [11–17]. Efficacy of the proposed methods in case of series and/or shunt compensated lines is not investigated by the authors in these papers.

There is very little reported work on the possibility of using DWT-based methods for the detection and classification of faults in lines with VSC-based FACTS controllers. In [18], DWT-based technique is employed to detect and classify faults in SSSC compensated lines. Fault location estimation results are shown for '3 phase fault' only, and the fault location is not measured accurately. Effect of fault resistance and operating mode of SSSC on the relay performance is not investigated. Wavelet entropy-based method is proposed for the detection and classification of lines compensated with SSSC and UPFC in [19], where signals from both ends are necessary. Fault location estimation is limited to before or after the location of FACTS controller, and exact fault location is not determined. Effect of fault resistance and operating modes of FACTS controller on the performance of wavelet-based relay is not investigated. Detection and classification of transmission line faults in the presence of STATCOM using wavelet-based summation index is discussed in [20]. However, fault location is not estimated and effect of fault resistance and change in operating mode of STATCOM on the relay performance are not investigated. Investigations carried out in [18–20] mainly focus on reactive power mode of FACTS controllers making use of multiple dedicated algorithms for fault detection, classification and fault location estimation. The impact of real power exchange capability of VSC-based FACTS controllers is not being reported and is carried out for the first time in this work. This main objective of this paper is to develop a new fast acting and reliable common wavelet transform-based relay logic for quick and accurate detection, classification of faults and accurately estimating fault location in transmission lines compensated with SSSC incorporating energy storage device which is immune to the operating mode of SSSC-ES and fault resistance. The paper is organized as follows. Details about the mathematical model of the study system and multi-resolution wavelet analysis are described in Sect. 2. Section 3 discusses the methodology used for the detection, classification and location of faults by the proposed wavelet transform-based relay. Simulation results for various fault types, locations, fault resistance and operating modes of SSSC are presented and analyzed in Sect. 4. Inference drawn from the study carried out and contributions of the present work are highlighted in Sect. 5.

2 System model

Figure 1 shows the hybrid series-compensated single machine connected to infinite bus (SMIB) system.

Here, 'X_t' is the reactance of transformer, $((R_L + j\,X_L) = (R_1 + R_2) + j\,(X_1 + X_2))$ is the net impedance of the line, 'Xc' is the capacitive reactance of series capacitor, and 'X_{sys}' is the system reactance on the infinite bus side. 'E_b' is the infinite bus voltage.

2.1 System equations

Figure 2 shows the circuit representation of a SSSC-ES. System is modeled in DQ frame of reference. Injected voltage by SSSC-ES is given by

$$V^i = \sqrt{V_Q^{i2} + V_D^{i2}} \tag{1}$$

where

$$V_D^i = K_m * V_{dc} * \mathrm{Sin}(\Phi + \gamma) \tag{2}$$

$$V_Q^i = K_m * V_{dc} * \mathrm{Cos}(\Phi + \gamma) \tag{3}$$

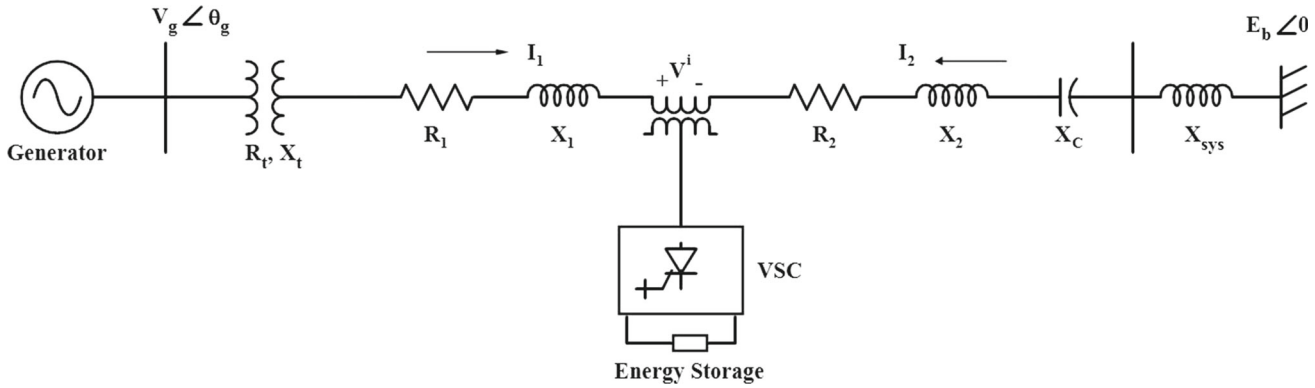

Fig. 1 Hybrid series-compensated system

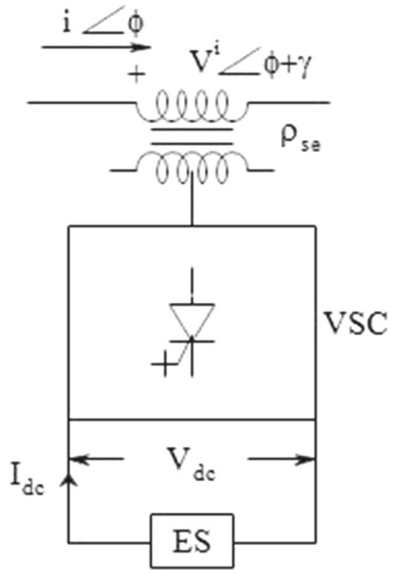

Fig. 2 Block schematic of SSSC-ES

where $K_m = K * \rho_{se} * \cos\beta$; $K = \frac{2\sqrt{6}}{\pi}$ for a 12-pulse converter, 'ρ_{se}' is the turns ratio of the transformer and

$$\Phi = \tan^{-1}\left(\frac{i_D}{i_Q}\right) \tag{4}$$

For better analysis, real (in phase) and reactive (quadrature) components of SSSC-ES are used.

$$V_P = V_D^i \mathrm{Sin}\Phi + V_Q^i \mathrm{Cos}\Phi \tag{5}$$

$$V_R = V_D^i \mathrm{Cos}\Phi - V_Q^i \mathrm{Sin}\Phi \tag{6}$$

It should be noted that a positive value of V_P signifies SSSC-ES drawing active power, and negative value indicates SSSC-ES supplying power. Similarly, negative value of V_R indicates capacitive mode and positive V_R implies inductive mode of operation of SSSC-ES.

Equations (7) and (8) are used to calculate 'γ' and 'β.' Phase angle of converter voltage,

$$\gamma = \tan^{-1}\left(\frac{V_{R(\mathrm{ord})}}{V_{P(\mathrm{ord})}}\right) \tag{7}$$

Dead angle,

$$\beta = \mathrm{Cos}^{-1}\left(\frac{\sqrt{V_{P(\mathrm{ord})}^2 + V_{R(\mathrm{ord})}^2}}{k * \rho_{se} * V_{dc}}\right) \tag{8}$$

Line current,

$$I = \sqrt{i_Q^2 + i_D^2} \tag{9}$$

For the system shown in Fig. 1, system equations are given by

$$V_{ga} = R_e i_a + L_e \frac{\mathrm{d}i_a}{\mathrm{d}t} + V_a^i + V_{ca} + E_{ba} \tag{10}$$

$$V_{gb} = R_e i_b + L_e \frac{\mathrm{d}i_b}{\mathrm{d}t} + V_b^i + V_{cb} + E_{bb} \tag{11}$$

$$V_{gc} = R_e i_c + L_e \frac{\mathrm{d}i_c}{\mathrm{d}t} + V_c^i + V_{cc} + E_{bc} \tag{12}$$

where $R_e = R_t + R_1 + R_2$ and $X_e = \omega_b L_e = X_t + X_1 + X_2 + X_{\mathrm{sys}}$.

Converting Eqs. 10, 11 and 12 to DQ using Kron's transformation [1], we get

$$\frac{\mathrm{d}i_Q}{\mathrm{d}t} = \frac{W_b}{X_l}\left[V_{gQ} - E_{bQ} - i_Q R_e + X_e i_D - V_Q^i - V_{cQ}\right] \tag{13}$$

$$\frac{\mathrm{d}i_D}{\mathrm{d}t} = \frac{W_b}{X_l}\left[V_{gD} - E_{bD} - i_D R_e - X_e i_Q - V_D^i - V_{cD}\right] \tag{14}$$

Voltage at the generator bus and the power generated by the generator are described by (15) and (16)

$$V_{gm} = \sqrt{V_{gQ}^2 + V_{gD}^2} \tag{15}$$

$$P_g = V_{gQ} * i_Q + V_{gD} * i_D \tag{16}$$

Equations (17) and (18) represent expressions for V_R and active power component of SSSC-ES, respectively.

$$-(X_{\text{SSSC}} * I) = V_D^i * \text{Cos}\varphi - V_Q^i * \text{Sin}\varphi \tag{17}$$

$$P = i_D * V_D^i + i_Q * V_Q^i \tag{18}$$

2.2 Operating modes and control strategy for SSSC-ES

When an energy storage device is connected at the DC bus of SSSC, operating range of SSSC covers all the four quadrants in *P–Q* plane. Various operating modes of SSSC-ES are

- *I quadrant* Inductive reactive power, absorbing real power.
- *II quadrant* Inductive reactive power, supplying real power.
- *III quadrant* Capacitive reactive power, supplying real power.
- *IV quadrant* Capacitive reactive power, absorbing real power.

A 150 MVA SSSC is considered for the analysis in the present work. Operating modes of SSSC-ES in the four quadrants are so considered that the voltage injected by SSSC is within the rated value (0.1681 pu).

In the case of SSSC with energy storage device, type 1 control is practiced to enable controlling both magnitude and phase angle of the converter output voltage [21]. The reference active and reactive voltages, $V_{\text{P(ord)}}$ and $V_{R\text{(ord)}}$ are used to calculate phase angle 'γ' and dead angle 'β' using Eqs. (7) and (8). Control strategy for SSSC-ES can be either to maintain injected voltage constant (Constant V_{P} and V_R) or to maintain impedance offered by SSSC-ES constant (Constant R_{SSSC} and X_{SSSC}) or constant real power control (Constant P). Constant emulated resistance and constant emulated reactance control strategy are adapted for SSSC in the present work.

2.3 Wavelet analysis

Fourier transform is the commonly used method to determine the frequency components present in the time-varying signal. However, it does not provide any information about the time at which these frequencies are present. Thus, it is not suitable for a non-stationary signal like fault current and voltage signals. Short-time Fourier transform gives both time and frequency information. Its limitation is fixed widow length. Small window length suffers from poor frequency resolution, and large widow length results in poor time resolution. A better alternative is to use wavelet transform to get information about frequency components present in the signal. It uses a varying window length, i.e., short window length for high frequencies and large window for small frequencies.

2.3.1 Mother wavelet and multi-resolution wavelet analysis

The first step in the wavelet analysis is selection of a proper mother wavelet. The transmission line faults are fast decaying and of short duration. A mother wavelet with short period is required for the analysis of such signals. Daubechies (DB) series mother wavelets are best suited for detecting transients associated with fault events as the associated transforms are fast, stable and accurate [22]. Hence, DB5 is considered as the mother wavelet in the present work.

Multi-resolution wavelet analysis decomposes the signal being analyzed into a low-frequency band called approximate coefficients (A_1) and a high-frequency band called detail coefficient (D_1). If 'fs' is the sampling frequency in Hz, then frequency band of A_1 component will be '0' to fs/4 while that of D_1 component will be fs/4 to fs/2. Wavelet decomposition process can be further extended. In the second level, A_1 component from level 1 will be decomposed into A_2 component with the frequency band 0 to fs/8 and D_2 with a frequency band of fs/8 to fs/4. Number of levels of decomposition is generally selected based on the frequency band of interest.

In the present work, sampling frequency used is 24 kHz, i.e., 400 samples per cycle. Multi-resolution discrete wavelet analysis of all the three current signals is carried out using DB5 mother wavelet. Detail coefficient at level 3 (frequency band of 1501–3000 Hz.) is used to determine the fault index and is used to detect classify and locate fault.

3 Methodology

3.1 Fault index

For a time-variant signal say $u\,(t)$, various signal norms are defined which are useful to discriminate between various operating modes of the governing system. For example, L_1 norm for the signal $u\,(t)$ is the integral of its absolute value given by

$$u_1 = \int_{-\infty}^{\infty} |u(t)| \mathrm{d}t \tag{19}$$

Higher-order norms are defined for the time-varying signal in a similar way.

For the discrete time signal say $u(n)$, L_1 norm is defined as

$$|u|_1 = \sum_{n=i}^{i+N} |u(n)| \tag{20}$$

where 'N' is the number of samples over a desired time period.

In the present work, L_1 norm for the reconstructed three-phase current signals using wavelet detail coefficients at level 3 is found to accurately detect, classify and locate line faults.

For the system considered, L_1 norm-based fault index for phase 'A' current is defined as,

$$I_{\text{afi}} = \sum_{n=1}^{N} |\text{DI}_{a3}(n)| \tag{21}$$

where DI_{a3} is the phase 'A' current, reconstructed using wavelet detail coefficients at level 3 and 'N' is the number of samples over one cycle of power–frequency.

In a similar way, fault index for phase 'B' and phase 'C' currents, I_{bfi} and I_{cfi} are determined.

3.2 Criteria for detection and classification of faults

Fault index values for all the three-phase currents are computed through simulation for normal condition and fault on the line at various locations and various operating modes of SSSC. A suitable threshold value is selected such that

- If the fault index of all the three-phase currents is less than the threshold, then it is identified as normal condition.
- If the fault index of all the three-phase currents is more than the threshold, then it is symmetrical fault.
- In case of unsymmetrical fault, fault index values of phase currents more than the threshold value are identified as faulty phase/phases and rest are healthy phase/phases.

3.3 Detection of ground faults

In order to determine whether the fault involves ground or not, zero-sequence component of current during fault is utilized.

DC offset in the fault current and voltage results in inaccurate measurement of fundamental component of voltage and current by discrete Fourier transform (DFT) algorithm. Various methods are proposed to eliminate the DC offset, like digital mimic filter [23], modified Fourier filter algorithm [24], and subtracting DC value at each sampling instant [25]. A simple and accurate digital mimic impedance-based filter is used in the present work to remove the DC offset from the fault current. DFT algorithm is used to determine the fundamental positive sequence components of I_a, I_b and I_c, i.e., I_{a1}, I_{b1}, and I_{c1}.

Zero-sequence component of current is determined as

$$I_0 = \frac{I_{a1} + I_{b1} + I_{c1}}{3} \tag{22}$$

The absence or negligible value of I_0 indicates that fault does not involve ground. Substantial value of I_0 means that fault involves ground.

3.4 Wavelet-based fault location estimator

Accurate estimation of fault location on transmission lines reduces the duration of line outage, labor and line maintenance costs. For known fault distances from the relay location, fault index values are obtained first through simulation. Using these values, a curve is plotted between fault index value and fault location. Fault distance from the relay point (Y) is estimated based on the best-fit (fourth-degree polynomial) equation obtained through curve fitting tool of MATLAB software, making use of fault index values (x). Accuracy of obtaining suitable polynomial equations and hence the accuracy of fault location estimation are improved by considering more values of fault index over the entire operating region of the relay for plotting the curve. The best-fit equations obtained for estimating fault location for symmetrical and unsymmetrical faults are given by Eqs. 23–26. Please note that in Eqs. 23–26, fault index values of phase 'B,' I_{bfi} is used to obtain the best-fit equation for fault location estimation, since in all the faults considered here, phase 'B' is a faulty phase. For other fault types, best-fit equations are obtained similarly utilizing the fault index values of one of the faulty phases. While obtaining the wavelet-based fault location estimator Eqs. 23–26, SSSC is bypassed. Impact of various operating modes of SSSC-ES on fault location estimation is discussed in Sect. 4.6.

Three-phase fault

$$Y = 21095x^4 - 23946x^3 + 10353x^2 - 2137.7x + 201.52 \tag{23}$$

LLG (ABG) fault

$$Y = 22606x^4 - 24423x^3 + 10039x^2 - 1978.9x + 181.23 \tag{24}$$

LL (AB) fault

$$Y = 44356x^4 - 35106x^3 + 10650x^2 - 1608.4x + 123.47 \tag{25}$$

LG (BG) fault

$$Y = 30559x^4 - 31709x^3 + 12458x^2 - 2319.7x + 196.79 \quad (26)$$

It should also be noted that the fault location estimation equations are valid for a given transmission line system. For any change in passive series compensation, coefficients of fault location estimator polynomial equations must be recalculated. However, in a hybrid series-compensated system shown in Fig. 1, reactance compensation by passive series capacitor is generally fixed and the percentage (level) of reactance compensation can be varied by varying the emulated reactance of SSSC. It is shown through case studies in Sect. 4 that, with the change in level of series compensation using SSSC, fault location estimator provides accurate distance of fault using the same coefficients of polynomial equations given by Eqs. 23–26.

Error in determination of fault determination is calculated as

$$\text{Error in } \% = \frac{\text{Estimated fault location} - \text{Actual fault location}}{\text{Line length}} \times 100 \quad (27)$$

3.5 Algorithm for detection, classification and estimation of fault location

- Select the required operating mode for SSSC-ES
- Obtain the three-phase current signals at the relay location.
- Decompose the current signals using multi-resolution wavelet analysis with DB5 mother wavelet.
- Use detail coefficients at level 3 to obtain L_1 norm fault index for all the three current signals.
- Compare the fault index values against the selected threshold values to detect and classify fault.
- Compute zero-sequence current and compare it with the selected threshold value to detect ground faults.
- Based on the detected fault type, use appropriate equation determined using wavelet-based fault index values to compute the distance of the fault from the relay location.
- When a fault is detected, compare the fault index value with the relay zone boundary threshold value for the detected fault type, to discriminate between within and outside zone faults.

4 Results

Fault index values are computed for the three-phase currents through simulation using Eq. (21) for normal (no fault) condition and fault condition. Simulation study is carried out for symmetrical and unsymmetrical faults at different locations and for various operating modes of SSSC using MATLAB/SIMULINK. Generator output power (P_g) is taken as 0.9 pu. A SSSC incorporating energy storage device can maintain the dc voltage constant, and in this analysis it is taken to be 0.7 pu. Net inductive reactance of the line, X_L is 1 pu. Capacitive reactance of passive series capacitor is fixed at 0.45 pu. Reactance emulated by SSSC, X_{SSSC} is varied between 0.15 pu (inductive) and − 0.15 pu (capacitive), so that net capacitive reactance compensation for the line is between 30 and 60%. It should be noted that negative value of X_{SSSC} implies that SSSC is operating in capacitive mode, and positive value of P_{ref} signifies that SSSC is absorbing real power from the network.

Table 1 Fault index values (in pu) under normal condition

Operating mode	I_{afi}	I_{bfi}	I_{cfi}
No SSSC	3.792×10^{-5}	3.792×10^{-5}	3.792×10^{-5}
With SSSC; $X_{SSSC} = -0.15$, $P_{ref} = 0.08$	3.825×10^{-5}	3.825×10^{-5}	3.825×10^{-5}

Table 2 Fault index values (in pu) during fault, fault at 25%

Fault type	I_{afi}	I_{bfi}	I_{cfi}
3 Ph. fault	0.076514	0.23015	0.154
LLG (ABG) fault	0.090151	0.21651	0.0013724
LL (AB) fault	0.15329	0.15334	8.3388×10^{-5}
SLG (BG) fault	0.002264	0.20751	0.0022612

4.1 No fault

It is seen from Table 1 that fault index values (in pu) during normal condition are negligibly small, and operating mode of SSSC has negligible impact on fault index values.

4.2 Fault at 25% line length from relay location

Symmetrical and unsymmetrical faults are simulated at 25% line length from relay location, at 1.5 s while SSSC is bypassed. Post-fault, fault index values obtained by considering detail coefficients at level 3 of I_a, I_b, and I_c for half a cycle after the occurrence of fault are shown in Table 2.

It is observed from Table 2 that post-fault, fault index values of the three-phase currents are quite small since these are per unit values. However, it is interesting to observe that post-fault, fault index values of faulty phases are substantially higher than the healthy phases which can be utilized to identify faulty phases.

Table 3 Fault index values (pu) during fault, fault at 75%

Fault type	I_{afi}	I_{bfi}	I_{cfi}	I_0
3 Ph. fault	0.015394	0.092466	0.10708	1.5432×10^{-8}
LLG fault	0.0041296	0.080765	0.00028015	0.27272
LL fault	0.038942	0.03897	6.7825×10^{-5}	5.1426×10^{-6}
SLG fault	0.00025174	0.081149	0.0002765	0.29282

4.3 Fault at 75% line length from relay location

4.3.1 Without SSSC

Symmetrical and unsymmetrical faults are simulated at a distance of 150 km, i.e., 75% line length without SSSC. Table 3 shows the fault index values during fault.

From Table 3, it is noted that the fault index values are substantially reduced when compared with fault at 25% (Table 2). This is because of the fact that as the distance of the fault from the relay location is increased, fault current is reduced and hence magnitude of the high-frequency component in the current signal is also reduced. From Table 3, it is also observed that the zero-sequence component of current is significant in case of ground faults.

4.3.2 With SSSC

Table 4 shows the obtained fault index with various operating modes of SSSC-ES. It is interesting to note that for a given fault type and location, the variation in fault index values is not very significant, corresponding to change in operating mode of SSSC. This is not surprising since SSSC injects balanced voltage and does not contribute significantly to the high-frequency components in the current signal.

4.4 Fault index threshold values for detection and classification of fault

In order to select a suitable threshold, to detect line fault and then to categorize fault, fault index values are obtained for all types of fault with all possible operating modes of SSSC-ES and at various distances on the line from the relay location. Detailed analysis of these values is performed, and threshold values are selected by determining maximum value of fault

Table 4 Impact of operating mode of SSSC on fault index values

Fault type	I_{afi}			I_{bfi}			I_{cfi}		
	$X_{SSSC} = -0.15$, $P_{ref} = 0$	$X_{SSSC} = 0$, $P_{ref} = 0.15$	$X_{SSSC} = -0.15$, $P_{ref} = -0.08$	$X_{SSSC} = -0.15$, $P_{ref} = 0$	$X_{SSSC} = 0$, $P_{ref} = 0.15$	$X_{SSSC} = -0.15$, $P_{ref} = -0.08$	$X_{SSSC} = -0.15$, $P_{ref} = 0$	$X_{SSSC} = 0$, $P_{ref} = 0.15$	$X_{SSSC} = -0.15$, $P_{ref} = -0.08$
3 Ph.	0.0155	0.0133	0.01673	0.0915	0.0959	0.0895	0.10626	0.10816	0.1055
LLG	0.0043	0.0048	0.00545	0.0799	0.0839	0.0780	0.00028	0.00026	0.00028
LL	0.0384	0.0418	0.0368	0.0385	0.0417	0.0369	10×10^{-5}	8.65×10^{-5}	12×10^{-5}
SLG	0.0002	0.00026	0.00024	0.0803	0.0840	0.0786	0.00027	0.00028	0.00027

Table 5 Estimated fault distance

Fault location (actual) in percentage	Estimated Fault location in percentage			
	Symmetrical fault	LLG fault	LL fault	LG fault
10	10.035	9.95	10.065	10.069
15	14.697	14.636	14.723	14.677
20	20.321	20.325	20.345	20.43
25	25.175	25.116	25.195	25.197
30	29.829	29.8	29.846	29.765
40	39.593	39.564	39.605	39.521
50	49.823	49.825	49.834	49.843
60	60.309	60.334	60.315	60.386
65	65.344	65.371	65.35	65.417
70	70.238	70.258	70.244	70.282
75	74.97	74.972	74.978	74.956
80	79.529	79.496	79.538	79.419
Maximum error (%)	− 0.471	− 0.504	− 0.462	− 0.581

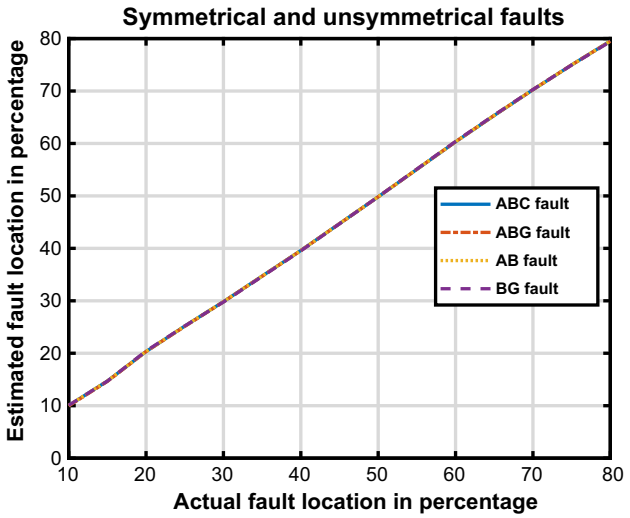

Fig. 3 Fault location estimation

index of healthy phases and minimum value of fault index for faulty phases.

Threshold values selected are: $I_{\text{tha}} = 40 \times 10^{-4}$, $I_{\text{thb}} = 40 \times 10^{-4}$ and $I_{\text{thc}} = 40 \times 10^{-4}$.

4.5 Fault location estimation

Using best-fit equations given by Eqs. 23–26, fault location is predicted for symmetrical and unsymmetrical faults.

Table 5 shows the estimated fault location for each fault type with SSSC operating in capacitive mode and absorbing real power (Xsssc $= -0.15$, $P_{\text{ref}} = 0.08$). Effect of other operating modes of SSSC-ES on fault location estimation is discussed in Sect. 4.6. It is very clear from Table 5 that the fault location estimation logic is able to compute the fault location with minimum error. Maximum error is found to be 0.581%.

Figure 3 shows the estimated fault location in the case of symmetrical and unsymmetrical faults. It is very clear from Fig. 3 that the wavelet transform-based fault location estimator estimates the fault location accurately, irrespective of the fault type.

4.6 Impact of operating mode of SSSC on estimation of fault location

Obtaining the best-fit equation to determine the fault location for each of the operating modes of SSSC is practically not feasible. Hence, irrespective of the operating mode of SSSC, Eqs. (23)–(26) are used for fault location estimation. Sample results obtained for various operating modes of SSSC in case of LLG (ABG) fault are shown in Table 6. It is interesting to note that error introduced due to change in operating mode of SSSC is insignificant. Similar results were obtained with other fault types, and the error in fault location estimation is negligible.

4.7 Discriminating internal and external faults using boundary condition threshold values

One of the major problems associated with distance relaying for the protection of transmission lines is the mal-operation of distance relay in the form of under-reach and over-reach. Operating mode of SSSC will modify the apparent impedance measured by distance relay during fault significantly, and thus chances of relay under-reach or over-reach are increased. In order to analyze the impact of operating mode of SSSC on proposed wavelet-based relay and to compare it with distance relay operation, reach of zone 1 unit of the proposed relay is considered as 80% from the relay location. In order to fix a threshold for fault index values corresponding to zone reach, fault index values are obtained for each of the fault type at 80% line length (zone boundary) for various operating modes of SSSC-ES and are shown in Table 7. It is observed from Table 7 that fault index values vary, though not significantly, with the change in operating mode of SSSC-ES. Hence, average value of fault index value for various operating modes of SSSC is used as the relay boundary threshold value to determine whether the fault is within or outside the zone reach. Boundary condition threshold values used are shown in the last column of Table 7.

Using these threshold values, relay logic is tested for the following operating modes of SSSC.

1. No SSSC

Table 6 Effect of operating mode of SSSC on fault location estimation

Fault location (actual) in percentage	Estimated fault location in percentage			
	No SSSC	$X_{\text{SSSC}} = -0.15$; $P_{\text{ref}} = 0$	$X_{\text{SSSC}} = 0$, $P_{\text{ref}} = -0.15$	Percentage maximum error
15	14.636	15.007	16.821	1.821
30	29.8	30.698	32.523	2.523
65	65.371	65.59	65.813	0.813
80	79.496	80.427	82.018	2.018

Table 7 Fault index threshold value for relay zone 1 reach

Fault type	Fault index				
	No SSSC	$X_{SSSC} = -0.15$, $P_{ref} = 0$	$X_{SSSC} = -0.1$, $P_{ref} = 0.05$	$X_{SSSC} = 0.05$, $P_{ref} = -0.15$	Average value
Symmetrical	0.086774	0.08554	0.087557	0.083968	0.08596
LLG (ABG)	0.075233	0.074135	0.076019	0.072361	0.074437
LL (AB)	0.034238	0.033624	0.035103	0.031295	0.033565
LG (BG)	0.076142	0.075073	0.076805	0.073647	0.075417

Table 8 Impact of operating mode of SSSC in discriminating internal and external faults

Fault type	Operating mode of SSSC	Wavelet-based Relay logic output				
		Fault at 78%	Fault at 79%	Fault at 80%	Fault at 81%	Fault at 82%
Symmetrical fault/LLG fault/LL fault/LG fault	No SSSC	Within zone 1	Within zone 1	Within zone 1	Outside zone 1	Outside zone 1
	$X_{SSSC} = -0.15$, $P_{ref} = 0$	Within zone 1	Within zone 1	Outside zone 1	Outside zone 1	Outside zone 1
	$X_{SSSC} = -0.1$, $P_{ref} = 0.06$	Within zone 1	Within zone 1	Within zone 1	Within zone 1	Outside zone 1
	$X_{SSSC} = 0.06$, $P_{ref} = -0.14$	Within zone 1	Outside zone 1	Outside zone 1	Outside zone 1	Outside zone 1

2. With SSSC; $X_{SSSC} = -0.15$, $P_{ref} = 0$
3. With SSSC; $X_{SSSC} = -0.1$, $P_{ref} = 0.06$
4. With SSSC; $X_{SSSC} = 0.06$, $P_{ref} = -0.14$

Output obtained from wavelet-based relay logic is shown in Table 8.

It is observed from Table 8 that the developed relay logic is able to correctly discriminate between within and outside zone faults in case of (1) No SSSC and (2) SSSC operating in capacitive mode. However, from Table 8, it is clear that the relay over-reaches (less than 2% over-reach) when SSSC is in capacitive mode and absorbing real power. Similarly, relay under-reaches (less than 2% under-reach) and does not operate when SSSC is in inductive mode and supplying real power. It is interesting to note that the amount of under-reach and over-reach (less than 2%) is not significant compared with more than 10% over-reach and under-reach expected with distance relays.

4.8 Impact of fault resistance (R_F) on relay operation

Setting of distance relay is usually done based on the positive sequence line impedance of the protected line length. However, fault resistance will have an impact on the measured impedance by the distance relay which may result in mal-operation of the relay. This can be avoided to a certain extent by accommodating the fault resistance in the setting of the distance relay. Selecting a suitable value for fault resistance is difficult since it varies with system voltage, line length, soil resistance, etc. Improper value of fault resistance used in distance relay setting will lead to mal-operation of distance relay.

With appropriate ratio of voltage and current inputs, a distance relay always measures positive sequence impedance between relay location and fault point [26]. In order to analyze the impact of fault resistance on wavelet transform-based relay, various test cases are considered with symmetrical and unsymmetrical faults on the line and with various operating modes of SSSC-ES. Results obtained are encouraging for the proposed wavelet-based relay logic. Sample results for two test cases are shown in Tables 9 and 10. Table 9 shows the results obtained for fault at 25% line length from relay location with SSSC bypassed, with conventional distance relay and wavelet transform-based relay. It is seen from Table 9 that the impedance measured by conventional distance relay is changed significantly with the increase in the value of R_F. This will result in inaccurate estimation of fault location and the operation of the distance relay is not reliable. However, with the proposed wavelet-based relay, fault index value and estimated value of fault location do not change significantly with increase in the value of R_F. Hence, the wavelet-based relay is more reliable.

Table 10 shows the impedance measured by the conventional distance relay and the output from wavelet-based relay when SSSC is included, is in the fault loop (fault at 75%) and operating in capacitive mode ($X_{SSSC} = -0.15$, $P_{ref} = 0$). It is observed that the conventional distance relay under-reaches and not operate when the value of R_F is increased. However, wavelet-based relay is least affected with the increase in value R_F and errors in estimation of fault location are negligible.

Table 9 Impact of fault resistance, fault at 25% line length

Fault type	R_F in Ω	Wavelet-based relay output		Distance relay output
		I_{bfi}	Estimated location in %	Zrelay in Ω
Symmetrical	0	0.23015	25.182	0.009937 + *j*0.2499
	2	0.2303	25.159	0.0241 + *j*0.24177
	5	0.23053	25.126	0.044511 + *j*0.23132
	10	0.2309	25.07	0.07598 + *j*0.21712
LLG (ABG)	0	0.2165	25.173	0.009969 + *j*0.2499
	2	0.21664	25.152	0.023197 + *j*0.24301
	5	0.21685	25.122	0.042666 + *j*0.23399
	10	0.21718	25.072	0.075684 + *j*0.21837
LL(AB)	0	0.15334	25.201	0.0099691 + *j*0.2499
	2	0.15345	25.181	0.023226 + *j*0.24279
	5	0.15361	25.153	0.042739 + *j*0.23347
	10	0.15388	25.105	0.075684 + *j*0.21837
SLG (BG)	0	0.20751	25.203	0.0097506 + *j*0.24931
	2	0.20763	25.184	0.019412 + *j*0.24387
	5	0.20781	25.157	0.033892 + *j*0.23663
	10	0.20812	25.111	0.059044 + *j*0.22758

Table 10 Impact of fault resistance, fault at 75% line length

Fault type	R_F in Ω	Wavelet-based relay output		Distance relay output
		I_{bfi}	Estimated location in %	Zrelay in Ω
Symmetrical	0	0.093082	74.511	*0.063484* + *j*0.67548
	2	0.093157	74.454	*0.02417* + *j*0.72522
	5	0.093268	74.369	− *0.028425* + *j*0.79654
	10	0.093452	74.229	− *0.095481* + *j*0.91866

4.9 Final Relay annunciation and trip signal generation

The developed wavelet-based relay logic is tested with 2400 test cases, considering all 10 possible fault types at different locations, five operating modes of SSSC and with four different values of R_F. Results obtained showed that the proposed relay logic is able to detect fault with 100% accuracy and identify faulty phases with 98.5% accuracy. Maximum error in fault location estimation is found to be 2.87%. Also the proposed relay is able to detect and classify faults very quickly. Wavelet coefficients corresponding to just half cycle of power–frequency, i.e., 8.33 ms after the occurrence of fault, are sufficient. Identification of faulty phases quickly helps in selective (only faulty phase/phases) pole tripping and auto-reclosing to enhance the stability of the system.

A sample output from the proposed relay logic for a double line-to-ground fault involving A and B phases at 79% line length with $R_F = 15\ \Omega$ is shown as follows. Operating mode of SSSC considered is capacitive mode and absorbing real power. It is interesting to note that even with a fault resistance of 15 Ω, the proposed relay logic is able to detect and classify fault correctly. It is also able to identify correctly that the fault is within zone 1 and error in determination of fault location is negligible.

```
Fault index values during fault
0.0059045 0.077819 0.00055308
Zero Sequence current 0.11677
Type of Fault: Unsymmetrical fault
Faulty Phases: A and B
Trip breaker poles 'A' and 'B' only
Fault involves ground!
Fault location in % y =77.347
Fault with in Zone1
```

5 Conclusion

A mathematical model for SSSC incorporating energy storage device is developed, and a new wavelet transform-based relay logic is proposed to quickly and accurately detect, classify faults and predict fault location in transmission lines compensated with SSSC incorporating energy storage device. L_1 norm fault index values are computed from

wavelet detail coefficients at level 3 to detect, classify faults, and best-fit equation is used to estimate the fault location. Wavelet transform-based boundary condition is utilized to discriminate between internal and external faults. Based on the results obtained from various case studies carried out, the following conclusions are drawn.

- The proposed wavelet transform-based relay logic detects and classifies short-circuit line faults with just wavelet coefficients of half a cycle of power–frequency, after the occurrence of fault, almost with 100% accuracy.
- Developed relay logic ensures that under-reach and over-reach of the relay are well within 2%.
- Wavelet transform-based fault location estimator predicts the fault location fairly accurately in the case of symmetrical and unsymmetrical faults, for various operating modes of SSSC-ES in all the four quadrants and is immune to change in the value of fault resistance.
- The developed relay logic makes use of common setting irrespective of the operating mode of SSSC-ES, and adaptive setting corresponding to change in operating mode is not necessary.

Appendix

Test system is adapted from IEEE first benchmark model.

System Data (All values in pu; Base MVA = 892.4, Base Voltage = 500 kV).

Generator data

$$\text{Ra} = 0;\ X_d = 1.79;\ X_q = 1.71;\ X'_d = 0.169;\ X''_d = 0.135;$$
$$X'_q = 0.228;\ X''_q = 0.2;\ T'_d = 0.4;\ T''_d = 0.0259;$$
$$T'_q = 0.1073;\ T''_q = 0.0463;\ f = 60;\ H = 5;\ D = 0;$$

Transmission system data

$$R_t = 0.0;\quad X_t = 0.14;\quad R_L = 0.04;\quad X_L = 1;$$
$$X_c = 0.45;\quad X_{\text{sys}} = 0.06;\quad V_g = V_g\angle\theta;\quad E_b = 1\angle 0;$$

SSSC data (150 MVA): Transformer tap = 1/6; $V_{\text{dc}} = 0.7$ pu.

References

1. Padiyar KR (2008) FACTS controllers in power transmission and distribution. New Age International, New delhi
2. Hingorani NG, Gyugyi L (2000) Understanding FACTS. IEEE Press, New York
3. Kasztenny B, Voloh I, Udren EA (2006) Rebirth of the phase comparison line protection principle. Presented at the 59th annual conference for protective relay engineers, TX
4. Singh RP (2007) Digital power system protection. PHI, New Delhi
5. Mohammadzadeh AH, Dabhagiyan Amiri I (2015) The impact of shunt FACTS devices on distance relay performance. In: 2nd IEEE international conference on knowledge-based engineering and innovation (KBEI)
6. Ghorbani A, Ebrahimi SY, Ghorbani M (2017) Active power based distance protection scheme in the presence of series compensators. Prot Control Mod Power Syst 2:7. https://doi.org/10.1186/s41601-017-0034-4
7. Singh AR, Dambhare SS (2013) Adaptive distance protection of transmission line in presence of SVC. Int J Electr Power Energy Syst 53(1):78–84
8. Dash PK, Pradhan AK, Panda G, Liew AC (2000) Adaptive relay setting for FACTS. IEEE Trans Power Deliv 15(1):38–43
9. Cruz M, Paz R, Chouty R, Bretas AS (2015) "Adaptive ground distance protection for UPFC compensated transmission lines: a formulation considering the fault resistance effect. Int J Electr Power Energy Syst 7:124–131
10. GururajaRao HV, Prabhu N, Mala RC (2019) Emulated reactance and resistance by a SSSC incorporating energy storage device. Int J Electr Comput Eng 9(2):840–850
11. Namdari F, Salehi M (2017) High-speed protection scheme based on initial current traveling wave for transmission lines employing mathematical morphology. IEEE Trans Power Deliv 32(1):246–253
12. Hu L, Qiu Y, Jiang L, Ren J, Wang S, Qi X, Wu J (2019) High voltage transmission line protection principle using transient signals. In: IOP conference series: earth and environmental science, vol 218, p 012065. https://doi.org/10.1088/1755-1315/218/1/012065
13. Valsan SP, Swamy KS (2009) Wavelet transform based digital protection for transmission lines. Int J Electr Power Energy Syst 31(7–8):379–388
14. Bharata Reddy J, Venkata Rajesh M, Mohanti D (2013) Robust transmission line fault classification using wavelet multi resolution analysis. Comput Electr Eng 39(4):1219–1227
15. Rathore B, Shaik AG (2017) Wavelet-alienation based transmission line protection scheme. IET Gener Transm Distrib 11(4):995–1003
16. Singh M, Panigrahi BK, Maeshwaran RP (2011) Transmission line fault detection and classification. In: International conference on emerging trends in electrical and computer technology
17. He Z, Fu L, Lin S, Bo Z (2010) Fault detection and classification in EHV transmission line based on wavelet singular entropy. IEEE Trans Power Deliv 25(4):2156–2163
18. Geetanjali M, Alias MA, Pandy TKS (2014) Discrete wavelet transform based fault detection and classification in a static synchronous series compensated transmission system. Adv Intell Syst Comput 258:85–94
19. El Zankoly AM, Desovic H (2011) Wavelet entropy based algorithm for fault detection and classification in FACTS compensated transmission lines. Int J Electr Power Energy Syst 33(8):1368–1374
20. Rao PV, Gefoor SA, Venkatesh C (2011) Detection of transmission line faults in the presence of STATCOM using wavelets. In: IEEE India conference, INDICON 2011
21. Gururaja Rao HV, Prabhu N, Mala RC (2015) Investigations on stability of a hybrid series compensated system with SSSC-ES. In: IEEE international conference on technological advancements in power and energy (TAPEnergy2015). Amrita School of Engineering, Kollam
22. Klomjit J, Ngaopitakkul A, Sreewirote B (2017) Comparison of mother wavelet for classification fault on hybrid transmission line systems. In: IEEE 8th international conference on awareness science and technology (iCAST), Taiwan
23. Kirpane R, Bedekar PP (2016) Removal of DC offset using digital mimic filtering technique. In: IEEE international conference on global trends in signal processing, information computing and communication

24. Yu S-L, Gu J-C (2001) Removal of decaying DC in current and voltage signals using a modified Fourier filter algorithm. IEEE Trans Power Deliv 16(3):372–379
25. Cho YS, Lee CK, Jang G, Lee HJ (2009) An innovative decaying DC component estimation algorithm for digital relaying. IEEE Trans Power Deliv 24(1):73–78
26. Oza BA, Nair NKC, Mehta RP, Makwana VH (2010) Power system operation and switchgear. TMH, New York